Synthesis of Energy-Bounded Planar Caging Grasps Using Persistent Homology

Jeffrey Mahler, *Member, IEEE*, Florian T. Pokorny, *Member, IEEE*, Sherdil Niyaz, *Member, IEEE*, and Ken Goldberg, *Fellow, IEEE*

(Invited Paper)

***Abstract*— For applications such as manufacturing, caging grasps restrict object motion without requiring complete immobilization, providing a robust alternative to force- and form-closure grasps. Energy-bounded cages are a new class of caging grasps that relax the requirement of complete caging in the presence of external forces such as gravity or constant velocity pushing in the horizontal plane with Coulomb friction. We address the problem of synthesizing planar energy-bounded cages by identifying gripper and force-direction configurations that maximize the energy required for the object to escape. We present Energy-Bounded-Cage-Synthesis-2-D (EBCS-2-D), a sampling-based algorithm that uses persistent homology, a recently-developed multiscale approach for topological analysis, to efficiently compute candidate rigid configurations of obstacles that form energy-bounded cages of an object from an α-shape approximation to the configuration space. If a synthesized configuration has infinite escape energy then the object is completely caged. EBCS-2-D runs in $O(s^3 + sn^2)$ time, where s is the number of samples and n is the number of object and obstacle vertices, where typically $n \ll s$. We observe runtimes closer to $O(s)$ for fixed n. We implement EBCS-2-D using the persistent homology algorithms toolbox and study performance on a set of seven planar objects and four gripper types. Experiments suggest that EBCS-2-D takes 2–3 min on a 6 core processor with 200 000 pose samples. We also confirm that an rapidly-exploring random tree* motion planner is unable to find escape paths with lower energy. Physical experiments on a five degree of freedom Zymark Zymate and ABB YuMi suggest that push grasps synthesized by EBCS-2-D are robust to perturbations. Data and code are available at http://berkeleyautomation.github.io/caging/.**

***Note to Practitioners*—For automation applications in manufacturing where object models are precisely known, "energy-bounded cages" are a robust approach to robot grasping in the presence of gravity or friction. This paper presents a synthesis algorithm for planar instances, where the object can be modeled as a planar extrusion and the motion occurs in the vertical or horizontal plane. We also present experiments with robots and a website with code and data.**

***Index Terms*— Computational geometry, motion planning, robots, topology.**

I. Introduction

IN MANUFACTURING, there are many applications where parts must be reliably grasped and moved without precise constaints on object pose (for example in kitting or logistics). Caging configurations, in which an object's mobility is bounded by a set of obstacles, can provide robustness to perturbations in object pose.

The standard model of caging (complete caging) considers whether a set of obstacles can be placed in a configuration such that the object cannot escape because its mobility is restricted to a bounded set in the free configuration space $\mathcal{F}$ [1], [2] as illustrated in the left part of Fig. 1. When an energy potential $U : \mathcal{C} \times \mathcal{C} \rightarrow \mathbb{R}$ specifying an energy field such as gravity is defined on the configuration space $\mathcal{C}$, the notion of caging can be generalized to *energy-bounded caging* [3], where the object is constrained to a bounded path-component of the subset of the free configuration space $\mathcal{F}$ with energy less than some threshold u. This arises, for example, when a constant force-field such as gravity acts on the object. We show that energy-bounded cages also occur in the context of constant velocity planar pushing with Coulomb friction.

This paper presents Energy-Bounded-Cage-Synthesis-2-D (EBCS-2-D), a sampling-based algorithm for synthesis of energy-bounded cages given a polygonal object and a rigid configuration of polygonal obstacles under a concave energy field defined over object translations, such as gravity or planar pushing. EBCS-2-D synthesizes an list of energy-bounded cages ranked by escape energy using persistent homology, a tool from computational topology that efficiently computes

Manuscript received July 10, 2017; accepted January 8, 2018. Date of publication May 16, 2018; date of current version July 2, 2018. This paper was recommended for publication by Associate Editors R. Alterovitz and K. Bekris and Editor S. Reveliotis upon evaluation of the reviewers' comments. This work was supported in part by the U.S. National Science Foundation through NRI under Award IIS-1227536, in part by the Department of Defense through the National Defense Science and Engineering Graduate Fellowship Program, in part by the Berkeley Deep Drive Program, in part by the Knut and Alice Wallenberg Foundation, and in part by Siemens, Google, Cisco, Autodesk, IBM, Amazon Robotics, and the Toyota Robotics Institute. *(Corresponding author: Jeffrey Mahler.)*

J. Mahler and S. Niyaz are with the Department of Electrical Engineering and Computer Science, University of California at Berkeley, Berkeley, CA 94705 USA (e-mail: jmahler@berkeley.edu; sniyaz@berkeley.edu).

F. T. Pokorny is with the RPL, School of Electrical Engineering and Computer Science, KTH Royal Institute of Technology, 114 28 Stockholm, Sweden (e-mail: fpokorny@kth.se).

K. Goldberg is with the Department of Industrial Engineering and Operations Research, University of California at Berkeley, Berkeley, CA 94705 USA, and also with the Department of Electrical Engineering and Computer Science, University of California at Berkeley, Berkeley, CA 94705 USA (e-mail: goldberg@berkeley.edu).

Color versions of one or more of the figures in this paper are available online at http://ieeexplore.ieee.org.

Digital Object Identifier 10.1109/TASE.2018.2831724

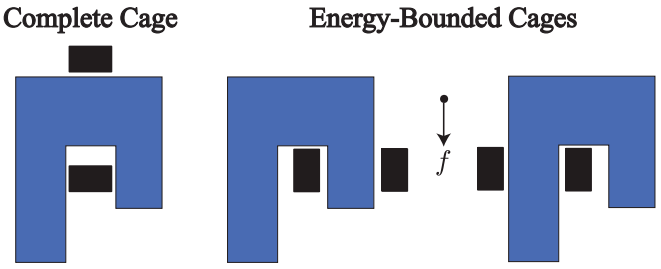

Fig. 1. Complete and energy-bounded cages. a complete cage (left). The blue object is constrained to a bounded component of the free configuration space by the rigid arrangement of the two gripper fingers (black). Two energy-bounded cages with respect to a force direction f, e.g., from gravity or constant velocity pushing with Coulomb friction (middle and right). The blue object is constrained by both the gripper and the force field. The rightmost configuration requires more energy to escape than the middle configuration.

representatives for bounded components of the free configuration over varying escape energy thresholds. EBCS-2-D constructs a weighted α-shape from samples of object poses and a lower bound on their penetration depth [3], finds a set of candidate energy-bounded cages using persistence, and prunes the candidates based on collisions and energy level. The escape energies returned by EBCS-2-D provably lower bound the true minimum escape energy for each returned cage. If the returned escape energy is infinite, then the object is completely caged.

We implement EBCS-2-D using the persistent homology algorithms toolbox (PHAT) [4] to efficiently identify the most robust energy-bounded cages. We evaluate EBCS-2-D on a set of seven polygonal parts with parallel-jaw grippers using a push energy field and use it to synthesize optimal push directions. In each case, rapidly-exploring random tree (RRT)* optimal path planning was unable to find an escape path with lower energy than the estimated lower bound within 120 s. We also use EBCS-2-D for planar pushing on a physical Zymark Zymate robot and ABB YuMi with the parallel-jaw grippers and confirm that configurations synthesized by EBCS-2-D successfully push objects on a planar worksurface.

II. Related Work

A. Complete Caging Versus Energy-Bounded Caging

The standard concept of caging, which we refer to as "complete" caging, was introduced by Kuperberg [5] and extended by Rimon and Blake [6]. Caging is distinct from complete immobilization of an object by means of form- or force-closure grasps [7], which depend on the local contact geometry. A complete cage of an object causes the object to be constrained to a bounded subset of its free configuration space and requires reasoning about global properties of the configuration space.

Early research on caging studied the caging condition for n points in the plane caging a planar object [1], [5]. Rimon and Blake [6] described the space of cages for a two-finger gripper with one degree of freedom. Sudsang and Ponce [8], [9] proposed the caging-based methods for manipulating polygonal objects by means of disc-shaped robots moving in the plane. Allen *et al*. [10] proposed an algorithm to find all two-finger cage formations of planar polygonal objects by two point fingers which was extended to equilateral three-fingered hands by Bunis *et al*. [11]. Vahedi and van der Stappen [2] studied the computation of two- and three-finger cages on polygons and used a classification into squeezing and stretching cages. Rodriguez *et al*. [12] established and studied caging as a prestage to force-closure grasping. Diankov *et al*. [13] demonstrated that caging grasps can be used to manipulate articulated objects such as door handles.

Recent research has focused on computing cages for specific object families or approximate algorithms due to the difficulty of computing the configuration space for complex gripper and object geometries. These lines of research have primarily focused on synthesizing caging grasps from features in the object surface [14], [15] (e.g., handles) using features of the object surface to rank potential caging configurations [16]. Other research has studied cell-based approximations of the configuration space based on sampling [17].

Mahler *et al*. [3] defined energy-bounded caging and presented energy-bounded cage analysis (EBCA)-2-D, an analysis algorithm that can provably lower bound the minimum escape energy to verify energy-bounded cages for a fixed object and obstacle configuration. The present paper proposes a synthesis algorithm, EBCS-2-D and considers energy-bounded cages in the context of planar pushing. This is an extended and revised version of "Synthesis of Energy-Bounded Planar Caging Grasps using Persistent Homology," which appeared at the Workshop on the Algorithmic Foundations of Robotics (WAFR) in December 2016 and was invited to the T-ASE special issue on WAFR. This version includes revised text, visualizations of persistence diagrams from real data, additional experiments evaluating energy-bounded cages for planar pushing with a physical ABB YuMi robot, and appendices for proofs and mathematical derivations.

B. Pushing for Manipulation

Mason [18] introduced the study of planar pushing to robotics and studied mechanics and planning problems for pushing operations [19]. Constant-velocity quasi-static planar pushing in the horizontal plane can be modeled by an energy potential. Peshkin and Sanderson [20] gave a method to find the locus of the centers of rotation of a planar object for all possible pressure distributions of the object on a planar worksurface. Planar pushing can reduce grasp uncertainty using mechanical compliance and can be used to orient parts [21]. Goldberg [22] gave the first complete algorithm for synthesizing a sequence of pushes to orient polygonal parts without sensory feedback. Lynch and Mason [23] investigated controllability of planar pushing, to determine whether an object can be moved between two configurations purely by pushing actions using point and line contacts. Dogar *et al*. [24] used a physics-based analysis of 2-D contact wrenches to compute push grasps in clutter and proposed a combinatorial search method to plan push grasps in [25]. Koval *et al*. [26] decomposed grasping policies into a pre and post contact strategy to reduce uncertainty during pushing actions preceding a grasp using a partially observable Markov decision process planner.

C. Motion Planning and Computational Topology

We utilize sampling and a discrete representation of the collision space using α-shapes to reason about cages, building

on previous work on motion planning and computational topology. Semialgebraic function representations of configuration space can be used to prove path nonexistence [27], but in practice can be prohibitively expensive to compute. Zhang *et al.* [28] utilized a rectangular cell decomposition of the configuration space to prove path nonexistence for motion planning by assigning cells to the collision space based on penetration depth. McCarthy *et al.* [29] used (weighted) α-shapes, a simplicial complex construction defined by Edelsbrunner [30], to represent the collision space from pose samples, and presented an algorithm that can prove path nonexistence. In our previous work [3], we showed that an α-shape-based approximation to the configuration space could be used to analyze a given object and obstacle configuration to check whether it is a complete or energy-bounded cage. The present paper also builds on recent advances in the topological data analysis [31] and the concept of *persistent homology* [32] to identify "voids" corresponding to cages. Other applications of persistent homology in robotics include robust methods for clustering trajectories [33] and for motion planning [34], [35].

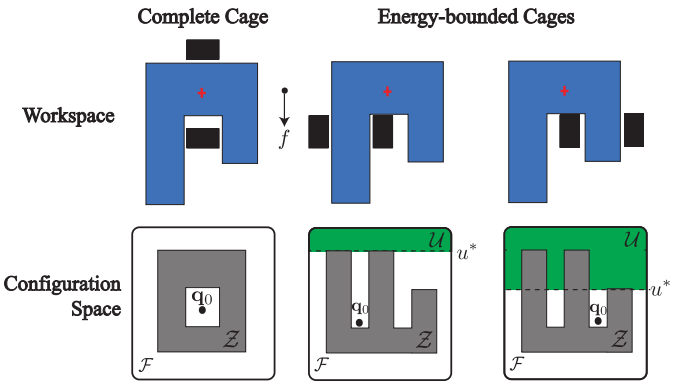

Fig. 2. Top row depicts gripper jaws $\mathcal{G}$ (in black) and an object $\mathcal{O}$ (in blue) in three configurations. The bottom row illustrates conceptually the corresponding point $\mathbf{q}_0 \in SE(2)$ in configuration space. While a complete cage corresponds to an initial pose $\mathbf{q}_0$ completely enclosed by forbidden space $\mathcal{Z}$, the energy-bounded cage on the right instead correpsonds to a case where $\mathbf{q}_0$ is enclosed by $\mathcal{Z}_u = \mathcal{Z} \cup \mathcal{U}(\mathbf{q}_0, u)$ where $\mathcal{U}(\mathbf{q}_0, u) = \{\mathbf{q} \in \mathcal{C} : U(\mathbf{q}, \mathbf{q}_0) > u\}$ for U that is strictly increasing with increasing vertical coordinate. The smallest value of u such that $\mathbf{q}_0$ is not enclosed is called the minimum escape energy, u^*.

III. Definitions and Problem Statement

Given a rigid polygonal object $\mathcal{O}$, a rigid configuration of obstacles $\mathcal{G}$ on a planar worksurface, and an energy function U, we consider the problem of finding and ranking the set of energy-bounded cages of $\mathcal{O}$ by $\mathcal{G}$.

A. Complete Caging and Energy-Bounded Caging

We consider a planar configuration space $\mathcal{C} \subseteq SE(2)$ of a compact polygonal planar object $\mathcal{O} \subset \mathbb{R}^2$ placed in a planar workspace with obstacles defined by fixed positions of a set of k polygons $\mathcal{G} = \mathcal{P}_1 \cup \ldots \cup \mathcal{P}_k \subset \mathbb{R}^2$, such as the jaws of a robot gripper. We assume the center of mass is known for both the object and obstacles. We denote the object polygon in pose $\mathbf{q} = (x, y, \theta) \in SE(2) = \mathbb{R}^2 \times \mathbb{S}^1$ relative to a reference pose $\mathbf{q}_0$ by $\mathcal{O}(\mathbf{q})$. We define the *collision space* of $\mathcal{O}$ relative to $\mathcal{G}$ by $\mathcal{Z} = \{\mathbf{q} \in SE(2) : int(\mathcal{O}(\mathbf{q})) \cap \mathcal{G} \neq \emptyset\}$ and denote by $\mathcal{F} = SE(2) - \mathcal{Z}$ the *free configuration space*.

We define the energy required to move the object between poses by an *energy function* $U : SE(2) \times SE(2) \to \mathbb{R}$ satisfying $U(\mathbf{q}, \mathbf{q}) = 0, \forall \mathbf{q} \in SE(2)$. This is consistent with [3], in which the reference pose was implicit in the energy function. For a fixed threshold $u \in \mathbb{R}$ and reference $\mathbf{q}_0 \in SE(2)$ define the *u-energy forbidden space* by $\mathcal{Z}_u(\mathbf{q}_0) = \mathcal{Z} \cup \{\mathbf{q} \in \mathcal{C} : U(\mathbf{q}, \mathbf{q}_0) > u\}$ and the *u-energy admissible space* $\mathcal{F}_u(\mathbf{q}_0) = SE(2) - \mathcal{Z}_u(\mathbf{q}_0)$. In this paper, we use the following definitions of caging [3] (see Fig. 2):

Definition (Complete and Energy-Bounded Caging): A configuration $\mathbf{q}_0 \in \mathcal{F}$ is completely caged if $\mathbf{q}_0$ lies in a bounded path-component of $\mathcal{F}$. We call $\mathbf{q}_0$ as a *u-energy-bounded cage of $\mathcal{O}$ with respect to U* if $\mathbf{q}_0$ lies in a bounded path-component of $\mathcal{F}_u(\mathbf{q}_0)$. Furthermore, the *minimum escape energy*, u^*, for an object $\mathcal{O}$ and obstacle configuration $\mathcal{G}$, is the infimum over values of u such that q is not a u-energy-bounded cage of $\mathcal{O}$, if a finite such u^* exists. Otherwise, we define $u^* = \infty$.

While energy-bounded cages can be defined for any energy function U, finding bounded components of $\mathcal{C}$ for all possible pairs of poses in the energy function may be computationally expensive. Thus, for synthesis, we require that the energy function can be derived from a univariate *potential function* $P : SE(2) \to \mathbb{R}$: $U(\mathbf{q}_i, \mathbf{q}_j) = P(\mathbf{q}_i) - P(\mathbf{q}_j)$. In this paper, we further assume that P depends only on the translational component $\mathbb{R}^2$ of $SE(2)$ and that P is concave on that space, which guarantees that the point of minimum potential within any convex set is on the boundary of the set. Given such an energy field U, the objective is to synthesize all energy-bounded cages $\mathbf{q}_i \in SE(2)$ with nonzero minimum escape energy.

B. Energy Functions

We now derive energy functions for gravity in the vertical plane and constant force pushing in the horizontal plane. We develop such functions based on the energy (mechanical work) that wrenches must exert to transport the object between two poses under a nominal wrench resulting from pushing or gravity.

1) Gravity in the Vertical Plane: Let m denotes the mass of the object. Then, the energy required to move the object from a reference configuration $\mathbf{q}_i$ to configuration $\mathbf{q}_j$ is $U(\mathbf{q}_j, \mathbf{q}_i) = mg\ (y_j - y_i)$, where $g = 9.81\ m/s^2$ is the acceleration due to gravity in the y-direction [3], [36]. This corresponds to the potential $P(\mathbf{q}) = mgy$.

2) Constant-Velocity Linear Pushing in the Horizonal Plane: Consider an object being pushed along a fixed direction $\hat{\mathbf{v}} \in \mathcal{S}^1$ by a gripper with a constant velocity on a horizonal worksurface under the quasi-static conditions and Coloumb friction with uniform coefficient of friction μ [18]–[20]. Then, the energy function $U(\mathbf{q}_j, \mathbf{q}_i) = F_p \hat{\mathbf{v}} \cdot\ (x_j - x_i, y_j - y_i) - \kappa$ is a lower bound on the energy required to move the object from pose $\mathbf{q}_i$ to $\mathbf{q}_j$ relative to $\mathcal{G}$, where $F_p \in \mathbb{R}$ is a bound on the possible resultant force due to contact between the object and gripper and $\kappa \in \mathbb{R}$ is a bound on the possible contact torques and frictional wrenches depending on the

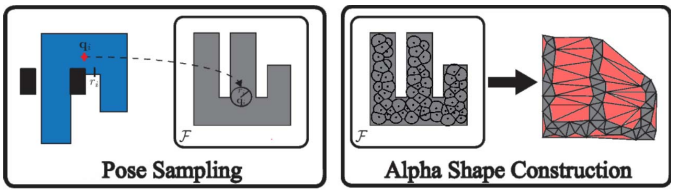

Fig. 3. We sample a set of poses Q and their penetration depth (left). An approximation of the forbidden space $\mathcal{Z} \subset SE(2)$ from Fig. 2 by unions of balls around sampled points Q results in an α-shape simplicial complex $A(X)$ (gray triangles) that is a subset of $\mathcal{Z}$ (right). The triangles of the weighted Delaunay triangulation $D(X)$ that are not in $A(X)$ approximate the free space (red triangles).

object geometry $\mathcal{O}$, the gripper geometry $\mathcal{G}$, and the friction coefficient μ. A justification is given in Appendix B. We use the linear potential $P(\mathbf{q}) = F_p \hat{\mathbf{v}} \cdot (x, y)$ to lower bound the minimum energy required for the object to escape under the nominal push wrench.

C. Configuration Spaces and α-Complexes

We utilize a family of simplicial complexes called α-complexes [30] to approximate the collision space $\mathcal{Z}$ and u-energy forbidden space [3]. For this purpose, we first uniformly sample a collection of s poses $Q = \{\mathbf{q}_1, \ldots, \mathbf{q}_s\}$, $\mathbf{q}_i = (x_i, y_i, \theta_i)$ in $\mathcal{Z}$ and determine the radius $r(\mathbf{q}_i) > 0$ for each $\mathbf{q}_i$, such that the metric ball $\mathbb{B}(\mathbf{q}_i) = \{\mathbf{q} \in SE(2) : d(\mathbf{q}, \mathbf{q}_i) \leq r(\mathbf{q}_i)\}$ is completely contained in $\mathcal{Z}$. These radii are computed using algorithms to lower bound the penetration depth [37] using the standard metric d on $SE(2)$; details can be found in [3]. The union of these balls $B(Q) = \cup_{i=1}^{s} \mathbb{B}(\mathbf{q}_i)$ forms a subset of the collision space that approximates $\mathcal{Z}$. See the left part of Fig. 3 for a conceptual illustration.

We can construct a cell-based approximation to $\mathcal{Z}$ using weighted α-shapes to guarantee that the cells are a subset of $\mathcal{Z}$. First, we follow the approach of [3] to lift samples from Q to a set $X \subset \mathbb{R}^3$ for computational reasons (see [3] for details). We then construct a weighted α-shape representation of $B(X)$ [30], [38] since the shape of the union of balls is difficult to analyze computationally.

Weighted α-shapes are a type of *simplicial complex*. A geometric k-simplex $\sigma = [\mathbf{v}_0, \ldots, \mathbf{v}_k]$ in $\mathbb{R}^d$ is a convex hull of $k+1$ ordered affinely independent elements $\mathbf{v}_0, \ldots, \mathbf{v}_k \in \mathbb{R}^d$ and a convex hull of an ordered subset of these elements is called a face τ of σ, indicated by $\tau \leq \sigma$. A finite simplicial complex $\mathcal{K}$ is a nonempty set of simplices such that if $\sigma \in \mathcal{K}$ and $\tau \leq \sigma$, then $\tau \in \mathcal{K}$ and if $\sigma, \sigma' \in \mathcal{K}$, then $\sigma \cap \sigma'$ is empty or an element of $\mathcal{K}$. In dimension 3, a simplicial complex $\mathcal{K}$ is a union of points, line segments, triangles, and tetrahedra whose intersections are either empty or another simplex in $\mathcal{K}$, thus generalizing the idea of both a graph and a triangulation in $\mathbb{R}^3$. The α-shape simplicial complex $A(X)$ corresponding to $B(X)$ lies strictly inside $B(X)$ and is homotopy equivalent to $B(X)$, meaning that topological properties of $B(X)$ can be computed directly from $A(X)$ [30]. In Addition, all simplices in $A(X)$ are contained in $D(X)$, the weighted Delaunay triangulation of X, a data structure that triangulates the convex hull of X. Fig. 3 provides a conceptual illustration.

D. Persistent Second Homology

Persistent homology [32] studies the topological features (e.g., holes, voids) that are created and destroyed over one parameter families of simplicial complexes called *filtrations*. Fig. 4 provides a conceptual visualization of 2-D slices of "voids" found by persistence for a 3-D filtration and a qualitative persistence diagram. A simplexwise filtration of a simplicial complex $K = \cup_{i=1}^{n} \sigma_i$ is a collection of simplicial complexes K_i such that $K_i = \cup_{i=1}^{i} \sigma_i$, so that K_{i+1} is the result of adding a single simplex σ_{i+1} to K_i. We call i as the filtration index. Such a filtration can arise naturally when a function $f : K \to \mathbb{R}$ is defined on the set simplices of K and simplices are ordered in decreasing values of f: $f(\sigma_i) \geq f(\sigma_j)$ for all $i \leq j$. Thus, persistence finds the topological features that emerge as the simplices are added in order of decreasing f. Here, $f(\sigma_i)$ is called the filtration value corresponding to filtration index i. The jth persistence diagram measures the dimension of the jth homology group $H_j(K_i)$ that corresponds to a vector space (with finite field coefficients). The dimension of each of these spaces is a topological invariant that does not vary under continuous deformations of the underlying simplicial complex $H(K_i)$. In this paper, we are interested in subcomplexes K_i of the weighted Delaunay triangulation $D(X) \subset \mathbb{R}^3$ and the *second homology group* $H_2(K_i)$. Regions of space that are completely enclosed by K_i correspond to components of $H_2(K_i)$ [39]. These voids in K_i can appear as we add new simplices with increasing i, or they can disappear as voids are filled in. The persistent second homology diagram enables us to visualize these topological changes. Each point (x, y) in the diagram corresponds to a pair of filtration indices (i, j) recording the fact that a void has "appeared" at index i and disappeared at index j. For a geometric simplicial complex, these index pairs (i, j) correspond to simplices (σ_i, σ_j), where σ_j is a *tetrahedron* (a three-simplex) which destroys or "fills in" a void, while σ_i corresponds to a *triangle* (2-simplex) that corresponds to the last complex needed to first create a fully enclosed void. The set of (i, j) pairs can be displayed in the (index)-persistence diagram, or alternatively, when the filtration arises from a function f, we may display the set of points $[f(\sigma_i), f(\sigma_j)]$. By considering the vertical distance $|f(\sigma_i) - f(\sigma_j)|$ from the diagonal, we can read off the parameter range of f during which a void exists in the evolution of the filtration.

IV. EBCS-2-D Synthesis Algorithm

EBCS-2-D (Fig. 5) takes as input a polygonal object $\mathcal{O}$, obstacle configuration $\mathcal{G}$, and continuous concave potential function P, and outputs a set of energy-bounded cages that require nonzero energy to escape.

Using uniform sampling, the algorithm first generates s object poses in collision $Q = \{\mathbf{q}_1, \ldots, \mathbf{q}_s\}$ and their corresponding penetration depths $R = \{r_1, \ldots, r_s\}$. We lift the poses to $\mathbb{R}^3$ and construct an α-shape approximation to the configuration space. Next, we construct a filtration by sorting

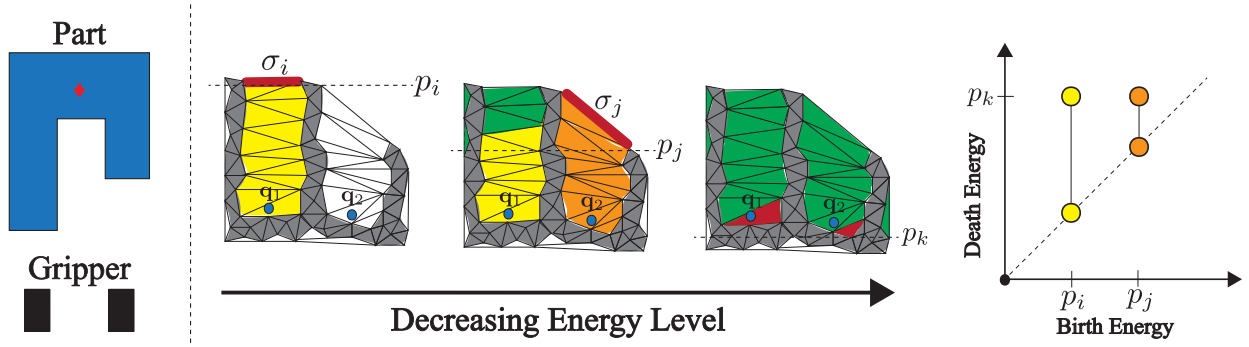

Fig. 4. Persistence diagram for ranking energy-bounded cages. Polygonal part and gripper polygons serve as input (left). We sample object poses X in collision and generate an α-shape representation (shown in gray in the three middle figures). Given an energy potential, we insert simplices in $D(X) - A(X)$ in decreasing order of energy potential, creating a filtration of simplicial complexes. Voids (yellow and orange) are born with the addition of edges σ_i and σ_j (red) at threshold potential levels p_i and p_j, respectively, and die with the additions of the last triangle in each void at potential p_k (red). The associated second persistence diagram reveals voids corresponding to energy-bounded cages. In particular, configuration $\mathbf{q}_1$ is persistent for a larger energy difference than configuration $\mathbf{q}_2$ (right). The escape energy of each configuration is equal to the difference in potentials: $u_1 = p_k - p_i$ and $u_2 = p_k - p_j$, and by the filtration ordering this implies that $\mathbf{q}_1$ has higher escape energy than $\mathbf{q}_2$.

all simplices in the free space in order of decreasing energy level and use persistent homology to identify path components that are bounded by the u-energy forbidden space. Finally, we examine the simplices within each bounded component in order of increasing energy to check for a collision-free object pose, and return the poses extracted from each component. Fig. 4 illustrates the use of persistence in our algorithm.

A. Filtrations and Persistence from Energy Functions

To synthesize energy-bounded cages with persistence, we first order the simplices of the α-shape approximation by decreasing energy level. We assumed that the potential $P : SE(2) \to \mathbb{R}^3$ depends only on the translational component $\mathbb{R}^2$ of $SE(2)$ and is concave on that space. In this case, for any k-simplex $\sigma = \text{Conv}(\mathbf{v}_0, \ldots, \mathbf{v}_k) \in D(X) - A(X)$ the maximum principle of convex optimization [40] implies that the minimum occurs on the boundary of the simplex, which is a vertex of σ since $\mathbb{R}^2$ is unbounded

$$\min_{\mathbf{x}\in\sigma} P(\pi(\mathbf{x})) = \min\{P(\pi(\mathbf{v}_0)), \ldots, P(\pi(\mathbf{v}_k))\}$$

where $\pi : \mathbb{R}^3 \to SE(2)$ denotes the projection to $SE(2)$. Using this fact, we construct a function $D(X) \to \mathbb{R}$

$$f(\sigma) = \begin{cases} \min_{\mathbf{x}\in\sigma} P(\pi(\mathbf{x})) & \sigma \in D(X) - A(X) \\ \infty & \sigma \in A(X). \end{cases}$$

This gives rise to a filtration $K = K(X, U) : \emptyset = K_0 \subset K_1 \subset \ldots \subset K_n \subset D(X)$ of simplices in $D(X)$ with respect to P as described in Section V-C, which we can use to find the bounded path-components corresponding to energy-bounded cages.

EBCS-2-D finds pairs of simplices σ_i, σ_j corresponding to the birth and death, respectively, of a bounded path-component $C(X) \subset D(X)$ in the free configuration space using persistent homology. All collision-free configurations within the bounded path-component are energy-bounded cages by definition. Therefore, EBCS-2-D next searches for the configuration $\mathbf{q} \in C(X) \cap \mathcal{F}$ with the highest minimum escape energy by iterating over the set of centroids of simplices in $C(X)$. While the set of simplex centroids only approximates $C(X) \cap \mathcal{F}$, in practice the centroids cover the space well due to the large number of samples used to construct the configuration space. The algorithm runs in $O(s^3 + sn^2)$ time, where s is the number of samples and n is the total number of object and obstacle vertices, since α-shape construction is $O(s^2 + sn^2)$ [3], [29] and the matrix reduction used in persistent homology is $O(s^3)$ in the worst case [41].

Input: Polygonal robot gripper $\mathcal{G}$, Polygonal object $\mathcal{O}$, Potential function P, Number of pose samples s
Output: $\hat{Q}$, set of energy-bounded cages with estimated escape energies

$Q = \varnothing, R = \varnothing, \ell = diam(\mathcal{G}) + diam(\mathcal{O})$; ▷ Initialize
$\mathcal{W} = [-\ell, \ell] \times [-\ell, \ell] \times [0, 2\pi)$;
for $i \in \{1, ..., s\}$ **do** ▷ Sample s poses in collision
  $\mathbf{q}_i = \text{RejectionSample}(\mathcal{W})$;
  $r_i = \text{LowerBoundPenDepth}(\mathbf{q}_i, \mathcal{O}, \mathcal{G})$;
  if $r_i > 0$ **then**
    $Q = Q \cup \{\mathbf{q}_i\}$, $R = R \cup \{r_i\}$;
  end if
end for
$X = \text{ConvertToEuclidean}(Q)$;
$D(X, R) = \text{WeightedDelaunayTriangulation}(X, R)$;
$A(X, R) = \text{WeightedAlphaShape}(D(X, R), \alpha = 0)$;
$K = \text{Filtration}(D(X, R), A(X, R))$;
$\Delta = \text{ComputeSecondHomologyPersistencePairs}(K)$;
for $(i, j) \in \Delta$ **do** ▷ Find energy-bounded cages
  $C(K_i, \sigma_j) = \text{PathComponent}(\sigma_j, K_i)$;
  if $\text{Bounded}(C(K_i, \sigma_j))$ **then**
    for $\sigma \in \text{Sorted}(C(K_i, \sigma_j)), P)$ **do**
      $\mathbf{q} = \text{Centroid}(\sigma)$;
      $u = P(\sigma_i) - P(\mathbf{q})$;
      if $\text{CollisionFree}(\mathbf{q})$ and $u > 0$ **then**
        $\hat{Q} = \hat{Q} \cup \{(\mathbf{q}, u)\}$;
      end if
    end for
  end if
end for
return $\hat{Q}$;

Fig. 5. EBCS-2-D.

B. Correctness

EBCS-2-D returns energy-bounded cages with a provable lower bound on the minimum escape energy:

Theorem 1: Let $\hat{Q} = \{(\hat{\mathbf{q}}_1, \hat{u}_1), \ldots (\hat{\mathbf{q}}_n, \hat{u}_n)\}$ denote the energy-bounded cages returned by EBCS-2-D. For each $(\hat{\mathbf{q}}_i, \hat{u}_i) \in \hat{Q}$, $\hat{\mathbf{q}}$ is a $\hat{u}$-energy bounded cage of $\mathcal{O}$ with respect to U.

A detailed proof is given in Appendix A.

C. Extension to Pushing

EBCS-2-D can be applied to push grasping in the horizontal plane. We use it to find push directions that yield robust energy-bounded cages by running EBCS-2-D for a set of sampled push directions using the constant velocity linear push energy of Section III-B. The extension runs EBCS-2-D using M push angles uniformly sampled from $[(\pi/2) - \varphi, (\pi/2) + \varphi]$ and returns a ranked list of push directions and energy-bounded cages that can be reached by a linear, collision-free path along the push direction. While the potential changes for each such push direction, the simplices only need to be re-sorted, and therefore, the sampling and α-complex construction only need to be performed once.

V. Experiments

We implemented EBCS-2-D in C++ and evaluated its performance on a set of polygonal objects under both gravitational and pushing energy fields. We used Computational Geometry Algorithms Library [42] to compute α-shapes, the Gilbert–Johnson–Keerthi Expanding Polytope Algorithm (GJK-EPA) algorithm of libccd [43] to compute penetration depth, and the twist reduction algorithm implemented in PHAT [4] to compute the second persistence diagram. Our data set consisted of seven polygonal parts created by triangulating the projections of models from Yale-CMU-Berkeley [44] and 3-DNet [45] onto a plane. All experiments ran on an Intel Core i7-4770K 350-GHz processor with six cores.

A. Energy Bounded Cages Under Linear Push Energy

We consider a linear push energy field with a push force bound of $F_p = 1.0$ for the set of parts with four grippers: rectangular parallel jaws, an overhead projection of a Zymark Zymate gripper with parallel jaws [46], an overhead projection of a Barrett hand with a pregrasping shape inspired by [25], and a four finger disc gripper inspired by [47]. We ran the pushing extension to EBCS-2-D for the rectangular parallel jaws, Zymark gripper, and Barrett hand with $s = 200\,000$ samples, an angle limit of $\varphi = (\pi/4)$, and $P = 5$ push directions to sweep from $-(\pi/4)$ to $(\pi/4)$ in intervals of $(\pi/8)$, and pruned all pushes with $\hat{u} < 0.5$ to ensure that our set of pushes was robust. For the four finger gripper, we ran EBCS-2-D with a fixed vertical push direction to illustrate the ability of our algorithm to prove complete cages. EBCS-2-D took approximately 170 s to run on average for a single push direction. Fig. 6 illustrates configurations synthesized by EBCS-2-D with the estimated minimum escape energy $\hat{u}$, which is the distance against the linear push energy that the object must travel to escape. To evaluate the lower bound of Theorem 1, we also used RRT* to attempt to plan an object escape path over the set of collision-free poses with energy less than $\hat{u}$, which was not able to find an escape path with energy less than $\hat{u}$ in 120 s of planning [3].

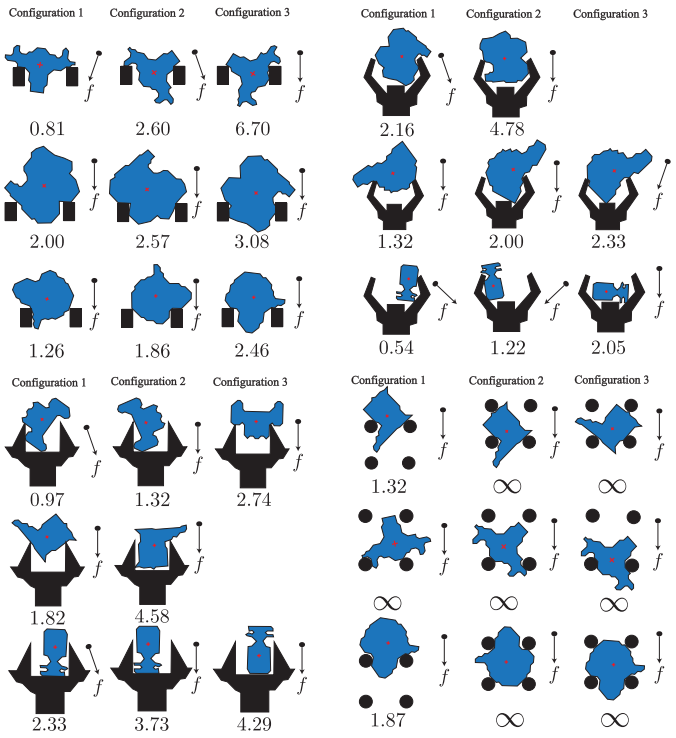

Fig. 6. Illustration of highest energy configurations and push directions synthesized using EBCS-2-D ranked from left to right for seven example polygonal objects (blue) and grippers (black) under a linear planar pushing energy field with a push force bound of $F_p = 1.0$. Displayed are three objects for each of the following grippers: (left-to-right, top-to-bottom) parallel-jaw grippers with rectangular jaws, a Barrett hand with fixed preshape, a Zymark Zymate gripper with fixed opening width, and a four finger disc gripper. Below each object the escape energy $\hat{u}$ estimated by EBCS-2-D using $s = 200\,000$ pose samples, which is the distance the object would have to travel against the pushing direction, and to the right is the synthesized push energy direction f. For each test case we searched over five energy directions from $-\pi/4$ to $\pi/4$ and checked push reachability as described in Section IV-C except for the four finger gripper, for which we ran only EBCS-2-D to illustrate complete cages. The energy of the synthesized configurations is not always proportional to the depth of part within the grippers, as suggested by the first row of results for the parallel jaw and Zymark gripper configurations. EBCA-2-D also synthesizes several complete cages for the four finger gripper.

B. Sample and Time Complexity

We also studied the sensitivity of the estimated escape energy for the highest energy configurations synthesized by EBCS-2-D for a fixed push direction and the algorithm runtime to the number of pose samples s.

Fig. 7 (left) shows the ratio of $\hat{u}$ for $s \in \{12.5, 25, 50, 100, 200, 400\} \times 10^3$ pose samples to $\hat{u}$ at $s = 400\,000$ pose samples for each of the displayed objects and gripper configurations. Fig. 7 (top) shows results using a parallel-jaw gripper and Fig. 7 (bottom) shows results with a Zymark Zymate gripper to illustrate sensitivity to the complexity of the polygonal gripper model. We averaged the ratios over five independent trials per value of s. Case A is only within 80% of the value at $s = 400\,000$ after $s = 200\,000$ samples, possibly

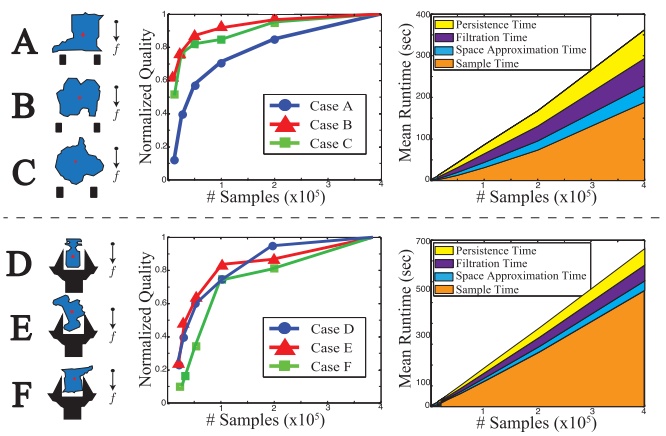

Fig. 7. Sample complexity of EBCS-2-D (middle). Plotted is the ratio of the highest minimum escape energy out of the energy-bounded cages synthesized by EBCS-2-D, $\hat{u}^*$, for the number of pose samples $s = \{12.5, 25, 50, 100, 200, 400\} \times 10^3$ on the object and gripper test cases displayed on the left. Performance is broken down by the polygonal gripper model used: parallel-jaw grippers (top) and a Zymark Zymate gripper (bottom). The mean runtime of EBCS-2-D in seconds is broken down by component of the algorithm for varying numbers of pose samples $s = \{12.5, 25, 50, 100, 200, 400\} \times 10^3$ (right). Each data point is averaged over five independent runs for each of the object and gripper configurations on the left. Despite the theoretical worst case s^3 runtime, the algorithm runtime is approximately linear in s, and is dominated by sampling time.

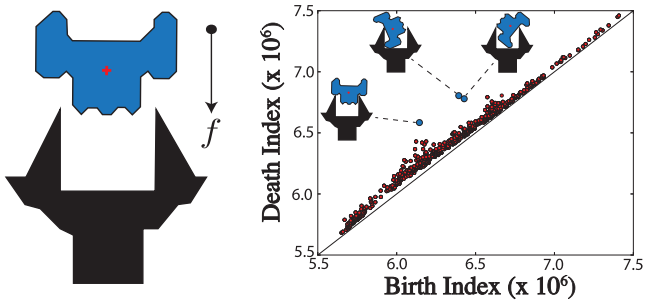

Fig. 8. Persistence diagram for the second homology persistence pairs (corresponding to "voids") in the filtration K identified during a run of EBCS-2-D with $s = 200\,000$ pose samples for a part (blue) and gripper configuration (black) with a vertical push force. The (i, j) coordinate for each point corresponds to the birth and death indices of the voids. Red points were pruned by our algorithm. Three blue points were identified by EBCS-2-D as energy-bounded cages, and their corresponding workspace configurations are illustrated next to the points. Note that the magnitude of differences between indices may not be indicative of the magnitude of energy differences between configurations.

because of the long thin portion of the configuration space as observed in [3]. Cases B and C both converge to within 95% after about $s = 200\,000$ samples. For cases D, E, and F with the complex Zymate gripper, all configurations require more samples to converge, possibly due to the thin portions of the gripper tips. The sample complexity is comparable to analysis of a single, fixed configuration with EBCA-2-D.

Fig. 7 (right) shows the relationship between the runtime of EBCS-2-D in seconds versus the number of pose samples s over five independent runs of the algorithm for the same objects. We broke down the run time by the section of the algorithm: sampling poses, constructing the α-shape to aproximate $\mathcal{C}$, sorting the simplices for the filtration, and computing and pruning candidate energy-bounded cages with persistence. The runtime is approximately linear in the number of pose samples, and the largest portion of runtime is the time to sample poses and compute penetration depth. This suggests that the runtime is considerably below the worst case s^3 scaling in practice. The persistence diagram computation in particular has been observed to commonly exhibit subquadratic runtime [41] despite its worst case cubic complexity. Runtime approximately doubles with the Zymate gripper due to an increase in sampling time, consistent with the quadratic time complexity of EBCS-2-D with respect to the number of object and obstacle vertices.

C. Persistence Diagrams

To further illustrate the notion of persistence, we study the persistence diagrams of the second homology group for a single object and the Zymark Zymate gripper in Fig. 8. To generate the diagram, we constructed the weighted Delauanay triangulation and α-shape using $s = 200\,000$ pose samples and examined the list Δ (generated on Line 14 of the EBCS-2-D pseudocode in Fig. 5). We see that the three energy-bounded cages returned by EBCS-2-D correspond to the three most persistent pairs, which appear furthest from the diagonal. Furthermore, our algorithm correctly rejects the large number of candidate configurations with very low persistence.

D. Physical Experiments

We evaluated the performance of energy-bounded cages synthesized by EBCS-2-D in pushing and grasping planar objects on two physical robots.

1) Known Object Pose: We evaluated the pushes synthesized by EBCS-2-D for the three object configurations on a Zymark Zymate robot with the Zymark gripper illustrated in Fig. 6 on a set of extruded fiberboard polygonal parts [46] to evaluate performance when the exact object pose is known, as is common in industrial automation. Fig. 9 (top) illustrates this experiment. For each configuration, the object was placed in the center of a turntable on a tepmlate to register the object pose, rotated to align the push direction with the arm's major axis, and pushed forward while the turntable oscillated with an amplitude of ± 0.1 rad to simulate external wrenches on the object. To test robustness, we added zero-mean Gaussian noise with standard deviation of 5 mm to the gripper translation and 0.04 rad to the gripper rotation in the plane. We then evaluated whether or not the object was captured and remained within the gripper jaws after being pushed 150 mm. Pushes planned by EBCS-2-D had a success rate of 100% versus 41% for a baseline of pushes planned by choosing gripper poses uniformly at random from (x, y) in the object bounding box and θ in $[0, 2\pi)$.

2) Image-Based Pose Registration: We also evaluated planar pushing on a set of six 3-D objects using an ABB YuMi with a parallel-jaw gripper using image-based registration to index a planned push from a database of pushes synthesized with EBCS-2-D to evaluate performance when the object pose is not known *a priori*. Fig. 9 (bottom) illustrates our experimental setup. First, we detected and segmented the each

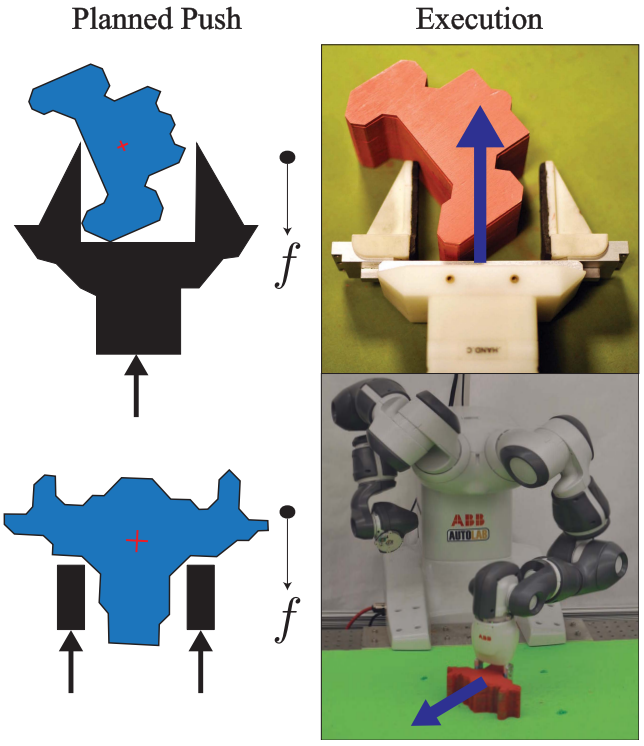

Fig. 9. Illustration of our experimental setups for executing energy-bounded cages synthesized with EBCS-2-D on a Zymark Zymate robot (top) and ABB YuMi robot (bottom). The Zymate was used to test performance when exact object pose was known and the YuMi was used to test performance when planning based on object segmentation masks in images. The synthesized planar configuration for each manipulator (left). The object remains in the gripper as it is pushed along a planar worksurface (right).

object from the background using color background subtraction with images from an overhead Primesense Carmine 1.08. We extruded and triangulated the segmentation masks and used EBCS-2-D to plan energy-bounded push-cages. To execute a planned push, the object was placed in the center of the planar worksurface by a human operator and the object was registered by minimizing the pixelwise difference between the new and original segmentation mask over all possible orientations. The robot then attempted to push the object 10 cm and lift the object by closing the jaws on the object after the attempted push. We added zero-mean Gaussian noise with standard deviation of 2.5 mm to the gripper translation in the plane to test robustness to perturbations.

Table I summarizes the performance of energy-bounded cages performed on the ABB YuMi for capturing the object (keeping it between the jaws), pushing the object 10 cm, and grasping and lifting the object. We evaluated each for four trials with the object rotated by $(\pi/2)$ on each trial, and we compared against the random baseline used in the Zymark Zymate experiments. The most common failure mode occurred when the parallel jaws contacted the object before reaching the target gripper configuration, suggesting that modeling uncertainty in the gripper approach could improve performance.

TABLE I

PERFORMANCE OF ENERGY-BOUNDED CAGES PLANNED BY EBCS-2-D FOR CAPTURING, PUSHING, AND GRASPING SIX PLANAR TEST OBJECTS FOR 14 TRIALS EACH ON AN ABB YUMI VERSUS THE PERFORMANCE OF A RANDOM BASELINE

Method	Captures (%)	Pushes (%)	Grasps (%)
Random	36	66	18
EBCS-2D	**98**	**79**	**86**

VI. DISCUSSION AND FUTURE WORK

We present EBCS-2-D, a synthesis algorithm for energy-bounded cages of polygonal objects and rigid configurations of obstacles under a 2-D energy field, and use EBCS-2-D to synthesize constant velocity planar pushes under Coulomb friction. In the future work, we will model uncertainty in gripper approach for pushing and explore caging as a prestage to force-closure grasping and stretching cages [2], [12]. We also plan to explore extensions of our algorithms to caging in 3-D and to study energy functions to model task-specific caging and fields due to electricity or magnetism.

APPENDIX A
CORRECTNESS OF EBCS-2-D

EBCS-2-D synthesizes energy-bounded cages of a polygonal object $\mathcal{O}$ by a rigid configuration of polygonal obstacles $\mathcal{G}$ with respect to a continuous energy function $U : SE(2) \times SE(2) \to \mathbb{R}$. We require that the energy function U can be derived from a univariate potential function $P(\mathbf{q}) : SE(2) \to \mathbb{R}$, $U(\mathbf{q}_i, \mathbf{q}_j) = P(\mathbf{q}_i) - P(\mathbf{q}_j)$. We refer to poses as $\mathbf{q} = (x, y, z) \in SE(2)$. See Fig. 5 for the EBCS-2-D pseudocode or Section III for further definitions.

Theorem 2 (Correctness of EBCS-2-D): Assume the object is specified as a compact polygon $\mathcal{O} \subset \mathbb{R}^2$ and the obstacles are defined a rigid configuration of a set of k polygons $\mathcal{G} = \mathcal{P}_1 \cup \ldots \cup \mathcal{P}_k \subset \mathbb{R}^2$. Furthermore, assume the energy function $U : SE(2) \times SE(2) \to \mathbb{R}$ satisfies the following.

1) $U(\mathbf{q}, \mathbf{q}) = 0$ for all $\mathbf{q} \in SE(2)$.
2) $U(\mathbf{q}_i, \mathbf{q}_j) = P(\mathbf{q}_i) - P(\mathbf{q}_j)$ for all $\mathbf{q} \in SE(2)$ and a potential function $P : SE(2) \to \mathbb{R}$.
3) P is continuous.
4) $P((x, y, \cdot)) = c$ for some $c \in \mathbb{R}$ (P does not depend on the orientation).
5) P is concave on the translational component $\mathbb{R}^2$.

Let $\hat{\mathcal{Q}} = \{(\hat{\mathbf{q}}_i, \hat{u}_i)\}_{i=1}^{N}$ be the list of poses returned by EBCS-2-D. For each $(\hat{\mathbf{q}}, \hat{u}) \in \hat{\mathcal{Q}}$, $\hat{\mathbf{q}}$ is a $\hat{u}$-energy bounded cage of $\mathcal{O}$ with respect to U.

Proof: It suffices to show that $(\hat{\mathbf{q}}, \hat{u})$ will only be added to the solution set $\hat{\mathcal{Q}}$ if $\hat{\mathbf{q}}$ is a $\hat{u}$-energy bounded cage of $\mathcal{O}$.

Lemma 3: Let $D(X, R)$ denotes the weighted Delaunay triangulation of the pose samples X and penetration depths R (computed on Line 11). Let $A(X, R) \subset D(X, R)$ denotes the weighted alpha shape of X and R at $\alpha = 0$ (computed on Line 12). Let π be the covering map defined in Section IV of [3]. Given any $p \in \mathbb{R}$, let $W_p(X, R) = \{\sigma \in D(X, R) \mid f(\sigma) > p\}$ denotes the *p-potential forbidden*

subcomplex of X, R, where

$$f(\sigma) = \begin{cases} \min_{x\in\sigma} P(\pi(x)) & \sigma \in D(X) - A(X) \\ \infty & \sigma \in A(X). \end{cases}$$

For any pose $\mathbf{q} \in SE(2)$ and $u \in \mathbb{R}$, let $p(\mathbf{q}) = u + P(\mathbf{q})$. Then, if $\mathbf{q} \in \mathcal{F}$ is in a bounded path-component of $\mathcal{C} - \pi(W_{p(\mathbf{q})}(X, R))$, $\mathbf{q}$ is a u-energy bounded cage of $\mathcal{O}$.

Proof: The p-potential forbidden subcomplex $W_{p(\mathbf{q})}(X, R) \subset V_u(X, R)(\mathbf{q})$ the *u-energy forbidden subcomplex* of X, R with respect to $\mathbf{q}$ defined in [3]. This is because $\forall\sigma \in W_{p(\mathbf{q})}(X, R)$, either $\sigma \in A(X, R) \Rightarrow \sigma \in V_u(X, R)(\mathbf{q})$ or $P(\sigma) > p(\mathbf{q}) \Leftrightarrow P(\mathbf{q}_i) > p(\mathbf{q})\ \forall \mathbf{q}_i \in \sigma \Leftrightarrow P(\mathbf{q}_i) - P(\mathbf{q}) = U(\mathbf{q}_i) > u$.

Recall that $\pi(V_u(X, R)(\mathbf{q})) \subset \mathcal{Z}_u$, the u-energy forbidden space defined in [3], and therefore $\mathcal{C} - \pi(W_{p(\mathbf{q})}(X, R)) \supset \mathcal{F}_u(\mathbf{q})$, the u-energy admissible space defined in [3]. Therefore any path in $\mathcal{C} - \pi(W_{p(\mathbf{q})}(X, R))$ can be restricted to $\mathcal{F}_u(\mathbf{q})$ which implies that $\mathbf{q}$ lies in a bounded path-component of $\mathcal{F}_u(\mathbf{q})$. Thus, by definition $\mathbf{q}$ is a u-energy-bounded cage. ∎

Now define the filtration $K(X, P) : \emptyset = K_0 \subset K_1 \subset \ldots \subset K_n \subset D(X, R)$ of simplices in $D(X, R)$ with respect to f. Let $\mathcal{I} = \{(i_m, j_m)\}_{m=1}^{M}$ denote the set of k persistence pairs for $K(X, P)$ such that $\dim(\sigma_{i_m}) == 2$. Then, any pair $(i, j) \in \mathcal{I}$ corresponds to the birth and death of a class of the second homology group H_2. We take this as an indication that $\pi(\sigma_k)$ lies in a bounded path-component $\pi(C(K_i, \sigma_j)) \subset \pi(D(X, R) - K_i)$ and additionally verify boundedness using a flood-fill algorithm [3], [29].

To verify that the component is bounded with respect to the $\hat{u}$ energy forbidden space, let $p = P(\sigma_i)$ and $u(\mathbf{q}) = P(\sigma_i) - P(\mathbf{q})$ for any $\mathbf{q} \in C(K_i, \sigma_j) \cap \mathcal{F}$, if such a pose exists. By the definition of the filtration, $K_i = W_p(X, R)$. By Lemma 3 any $\mathbf{q} \in C(K_i, \sigma_j) \cap \mathcal{F}$ is in a bounded path-component and is, therefore, a $u(\mathbf{q})$-energy-bounded cage of $\mathcal{O}$. EBCS-2-D only returns $\mathbf{q}, u$ for $u = P(\sigma_i) - P(\mathbf{q})$ (Line 19) if $\mathbf{q}$ is collison free (Line 20) and in the same bounded path-component as σ_j (Line 16). Therefore, $\hat{\mathbf{q}}$ is a $\hat{u}$-energy-bounded cage of $\mathcal{O}$ with respect to U.

Appendix B
Energy Function for Constant Velocity Quasi-Static Planar Pushing

Consider a compact polygonal object $\mathcal{O} \subset \mathbb{R}^2$ of mass m_O and a rigid configuration of a set of k polygonal obstacles $\mathcal{G} = \mathcal{P}_1 \cup \ldots \cup \mathcal{P}_k \subset \mathbb{R}^2$ of total mass m_G. Let $m = m_O + m_G$ be the total mass. Denote by $\mathbf{q} \in SE(2)$ the pose of $\mathcal{O}$ relative to the reference frame of $\mathcal{G}$. Assuming quasi-static conditions and a Coloumb friction model, let the object and gripper rest on a horizontal worksurface under gravity with a uniform coefficient of friction between the gripper, object, and surface: $\mu \in \mathbb{R}$. Assume a uniform pressure distribution for both $\mathcal{O}$ and $\mathcal{G}$ and let the center of mass of each be located at the centroid of the respective pressure distributions. Assume that the magnitude of any external wrench $w_e = (f_e, \tau_e)$ on the object is bounded by a constant λ.

Now, let $\mathcal{G}$ move along a fixed direction $\hat{v} \in \mathcal{S}^1$ with constant translational velocity of magnitude $\beta \in \mathbb{R}$ and zero angular velocity. Zero net force must be acting on $\mathcal{G}$ and $\mathcal{O}$ to maintain this velocity, and therefore, the force due to pushing f_p is equal and opposite of the forces due to friction f_f and forces due to external perturbations f_e. Thus, the pushing force is bounded by the maximum force due to friction and maximum magnitude of external wrenches: $\|f_p\|_2 \leq \mu Mg + \lambda$. This force may be applied to $\mathcal{O}$ through contact with $\mathcal{G}$, and therefore f_p may exert a torque τ_p on $\mathcal{O}$ relative to $\mathcal{G}$ such that $\tau_p \leq \rho f_p$, where $\rho \in \mathbb{R}$ is the maximum moment arm of $\mathcal{O}$ [18]–[20].

To derive the energy function, consider the amount of energy (mechanical work) that the time-varying external wrench $w_e(t) = (f_e(t), \tau_e(t))$ would have to exert to move $\mathcal{O}$ along a continuous path $\gamma : [0, 1] \to SE(2)$ from pose $\mathbf{q}_i$ to $\mathbf{q}_j$ (e.g., $\gamma(0) = \mathbf{q}_i, \gamma(1) = \mathbf{q}_j$) with a constant speed η under the pushing wrench $w_p = (f_p, \tau_p)$ and time-varying wrenches due to friction $w_f(t) = (f_f(t), \tau_f(t))$ [36]

$$\mathcal{E}(w_e) = \int_0^1 w_e(t) \cdot \dot{\gamma}(t) dt.$$

By the constant speed assumption, the kinetic energy of the object does not change. Therefore, the net work done on the object over the path γ is zero due to conservation of energy

$$\begin{aligned} \mathcal{E}(w_e + w_p + w_f) &= \int_0^1 (w_e(t) + w_p + w_f(t)) \cdot \dot{\gamma}(t) dt = 0 \\ &\Rightarrow \mathcal{E}(w_e) = -\mathcal{E}(w_p + w_f). \end{aligned}$$

We can upper bound the amount of work done by the constant pushing wrench w_p and time-dependent frictional wrench w_f using Cauchy-Schwarz

$$\begin{aligned} \mathcal{E}(w_p + w_f) &= \int_0^1 w_p \cdot \dot{\gamma}(t) dt + \int_0^1 w_f(t) \cdot \dot{\gamma}(t) dt \\ &= w_p \cdot \int_0^1 \dot{\gamma}(t) dt + \int_0^1 w_f(t) \cdot \dot{\gamma}(t) dt \\ &\leq (\mu Mg + \lambda)\hat{\mathbf{v}} \cdot (\mathbf{x}_j - \mathbf{x}_i) \\ &\quad + \rho\ (\mu Mg + \lambda)(\theta_j - \theta_i) \\ &\quad + \mu Mg \int_0^1 \|\dot{\gamma}(t)\|_2\ dt \text{ (by Cauchy-Schwarz)} \\ &\leq (\mu Mg + \lambda)\hat{\mathbf{v}} \cdot (\mathbf{x}_j - \mathbf{x}_i) \\ &\quad + 2\pi\rho\ (\mu Mg + \lambda) + \eta\mu Mg. \end{aligned}$$

And therefore, under our assumptions, we can lower bound the energy exerted by any external wrenches by

$$\begin{aligned} U(\mathbf{q}_j, \mathbf{q}_i) &= F_p \hat{\mathbf{v}} \cdot (\mathbf{x}_j - \mathbf{x}_i) - \kappa(\mathcal{O}, \mathcal{G}, \mu) \\ F_p &= -(\mu Mg + \lambda) \\ \kappa(\mathcal{O}, \mathcal{G}, \mu) &= 2\pi\rho\ (\mu Mg + \lambda) + \eta\mu Mg. \end{aligned}$$

This motivates our use of the linear, univariate potential $P(\mathbf{q}) = F_p \hat{\mathbf{v}} \cdot (\mathbf{x}_j - \mathbf{x}_i)$.

Appendix C
Numeric Issues in Implementation

In order for EBCS-2-D to be correct, the computed penetration depth r_i for a pose $\mathbf{q}_i$ must not be greater than the true 2-D generalized penetration depth, $r_i \leq p(\mathbf{q}_i)$. This can be

theoretically achieved using the lower bound algorithm given by Zhang *et al*. [28] by taking the maximum of the exact penetration depth between pairs of convex pieces in a convex decomposition of the object and obstacles, where the exact penetration depth can be computed with the GJK-EPA [48]. However, in practice GJK-EPA computes the exact penetration depth up to some tolerance $\pm\epsilon$. Thus to avoid misidentifying a configuration as a complete or energy-bounded cage, in practice, we use $r_i = \max(\hat{r}_i - \epsilon, 0)$, where $\hat{r}_i$ is the penetration depth computed using the algorithm of Zhang *et al*. [28]. To avoid futher numeric issues related to imprecision in the convex decomposition, computation of the maximum moment arm, or the triangulation, in practice it may be beneficial to additionally multiply the returned penetration depth by some shrinkage factor $0 < \nu < 1$, $r_i = \nu\max(\hat{r}_i - \epsilon, 0)$.

ACKNOWLEDGMENT

This paper was performed at the Autolab at University of California at Berkeley in affiliation with the AMPLab, Berkeley Artificial Intelligence Research, and the Center for Innovation Technology Research in the Interest of Society "People and Robots" Initiative: http://robotics.citris-uc.org. The authors would like to thank the anonymous WAFR reviewers for valuable feedback and the colleagues who provided helpful suggestions, in particular S. Bhattacharya, A. Garg, D. Gealy, S. Krishnan, M. Laskey, J. Liang, Z. McCarthy, S. McKinley, L. Miller, and A. Frank van der Stappen.

REFERENCES

[1] E. Rimon and J. W. Burdick, "Mobility of bodies in contact. I. A 2nd-order mobility index for multiple-finger grasps," *IEEE Trans. Robot. Autom.*, vol. 14, no. 5, pp. 696–708, Oct. 1998.

[2] M. Vahedi and A. F. van der Stappen, "Caging polygons with two and three fingers," *Int. J. Robot. Res.*, vol. 27, nos. 11–12, pp. 1308–1324, 2008.

[3] J. Mahler, F. T. Pokorny, Z. McCarthy, A. F. van der Stappen, and K. Goldberg, "Energy-bounded caging: Formal definition and 2-D energy lower bound algorithm based on weighted alpha shapes," *IEEE Robot. Autom. Lett.*, vol. 1, no. 1, pp. 508–515, Jan. 2016.

[4] U. Bauer, M. Kerber, and J. Reininghaus, "PHAT—Persistent homology algorithms toolbox," vol. 68, pp. 76–90, Jan./Feb. 2013. [Online]. Available: https://code.google.com/p/phat/

[5] W. Kuperberg, "Problems on polytopes and convex sets," in *Proc. DIMACS Workshop Polytopes*, 1990, pp. 584–589.

[6] E. Rimon and A. Blake, "Caging 2D bodies by 1-parameter two-fingered gripping systems," in *Proc. IEEE Int. Conf. Robot. Autom. (ICRA)*, Apr. 1996, pp. 1458–1464.

[7] R. M. Murray, Z. Li, and S. S. Sastry, *A Mathematical Introduction to Robotic Manipulation*. Boca Raton, FL, USA: CRC Press, 1994.

[8] A. Sudsang and J. Ponce, "On grasping and manipulating polygonal objects with disc-shaped robots in the plane," in *Proc. IEEE Int. Conf. Robot. Autom. (ICRA)*, May 1998, pp. 2740–2746.

[9] A. Sudsang and J. Ponce, "A new approach to motion planning for disc-shaped robots manipulating a polygonal object in the plane," in *Proc. IEEE Int. Conf. Robot. Autom. (ICRA)*, vol. 2. Apr. 2000, pp. 1068–1075.

[10] T. F. Allen, J. W. Burdick, and E. Rimon, "Two-finger caging of polygonal objects using contact space search," *IEEE Trans. Robot.*, vol. 31, no. 5, pp. 1164–1179, Oct. 2015.

[11] H. A. Bunis, E. D. Rimon, Y. Golan, and A. Shapiro, "Caging polygonal objects using equilateral three-finger hands," *IEEE Robot. Autom. Lett.*, vol. 2, no. 3, pp. 1672–1679, Jul. 2017.

[12] A. Rodriguez, M. T. Mason, and S. Ferry, "From caging to grasping," *Int. J. Robot. Res.*, vol. 31, no. 7, pp. 886–900, 2012.

[13] R. Diankov, S. S. Srinivasa, D. Ferguson, and J. Kuffner, "Manipulation planning with caging grasps," in *Proc. 8th IEEE-RAS Int. Conf. Humanoid Robots Humanoids*, Dec. 2008, pp. 285–292.

[14] F. T. Pokorny, J. A. Stork, and D. Kragic, "Grasping objects with holes: A topological approach," in *Proc. IEEE Int. Conf. Robot. Autom. (ICRA)*, Karlsruhe, Germany, May 2013, pp. 1100–1107.

[15] T. H. Kwok *et al.*, "Rope caging and grasping," in *Proc. IEEE Int. Conf. Robot. Autom. (I CRA)*, May 2016, pp. 1980–1986.

[16] T. Makapunyo, T. Phoka, P. Pipattanasomporn, N. Niparnan, and A. Sudsang, "Measurement framework of partial cage quality based on probabilistic motion planning," in *Proc. IEEE Int. Conf. Robot. Autom. (ICRA)*, May 2013, pp. 1574–1579.

[17] W. Wan and R. Fukui, "Efficient planar caging test using space mapping," *IEEE Trans. Autom. Sci. Eng.*, vol. 15, no. 1, pp. 278–289, Jan. 2016.

[18] M. T. Mason, *Mechanics of Robotic Manipulation*. Cambridge, MA, USA: MIT Press, 2001.

[19] M. T. Mason, "Mechanics and planning of manipulator pushing operations," *Int. J. Robot. Res.*, vol. 5, no. 3, pp. 53–71, 1986.

[20] M. A. Peshkin and A. C. Sanderson, "The motion of a pushed, sliding workpiece," *IEEE J. Robot. Autom.*, vol. RA-4, no. 6, pp. 569–598, Dec. 1988.

[21] S. Akella and M. T. Mason, "Parts orienting by push-aligning," in *Proc. IEEE Int. Conf. Robot. Autom.*, vol. 1. May 1995, pp. 414–420.

[22] K. Y. Goldberg, "Orienting polygonal parts without sensors," *Algorithmica*, vol. 10, no. 2, pp. 201–225, 1993.

[23] K. M. Lynch and M. T. Mason, "Controllability of pushing," in *Proc. IEEE Int. Conf. Robot. Autom.*, vol. 1. May 1995, pp. 112–119.

[24] M. Dogar, K. Hsiao, M. Ciocarlie, and S. Srinivasa, "Physics-based grasp planning through clutter," in *Proc. Robot., Sci. Syst. VIII*, 2012, pp. 78–85.

[25] M. Dogar and S. Srinivasa, "A framework for push-grasping in clutter," in *Proc. Robot., Sci. Syst. VII*, vol. 1. 2011.

[26] M. C. Koval, N. S. Pollard, and S. S. Srinivasa, "Pre-and post-contact policy decomposition for planar contact manipulation under uncertainty," *Int. J. Robot. Res.*, vol. 35, nos. 1–3, pp. 244–264, 2016.

[27] S. M. LaValle, *Planning Algorithms*. Cambridge, U.K.: Cambridge Univ. Press, 2006.

[28] L. Zhang, Y. J. Kim, and D. Manocha, "Efficient cell labelling and path non-existence computation using c-obstacle query," *Int. J. Robot. Res.*, vol. 27, nos. 11–12, pp. 1246–1257, 2008.

[29] Z. McCarthy, T. Bretl, and S. Hutchinson, "Proving path non-existence using sampling and alpha shapes," in *Proc. IEEE Int. Conf. Robot. Autom. (ICRA)*, May 2012, pp. 2563–2569.

[30] H. Edelsbrunner, "Weighted alpha shapes," Ph.D. dissertation, Dept. Comput. Sci., Univ. Illinois Urbana-Champaign, Urbana, IL, USA, 1992.

[31] G. Carlsson, "Topology and data," *Bull. Amer. Math. Soc.*, vol. 46, no. 2, pp. 255–308, 2009.

[32] H. Edelsbrunner and J. Harer, "Persistent homology—A survey," *Contemp. Math.*, vol. 453, pp. 257–282, Feb. 2008.

[33] F. T. Pokorny, M. Hawasly, and S. Ramamoorthy, "Multiscale topological trajectory classification with persistent homology," in *Proc. Robot., Sci. Syst.*, Jul. 2014. [Online]. Available: http://www.roboticsproceedings.org/rss10/p54.html

[34] F. T. Pokorny and D. Kragic, "Data-driven topological motion planning with persistent cohomology," in *Proc. Robot., Sci. Syst.*, Rome, Italy, Jul. 2015. [Online]. Available: http://www.roboticsproceedings.org/rss11/p49.html

[35] S. Bhattacharya, R. Ghrist, and V. Kumar, "Persistent homology for path planning in uncertain environments," *IEEE Trans. Robot.*, vol. 31, no. 3, pp. 578–590, Mar. 2015.

[36] D. C. Giancoli, *Physics: Principles With Applications*. London, U.K.: Pearson Education, 2005.

[37] L. Zhang, Y. J. Kim, G. Varadhan, and D. Manocha, "Generalized penetration depth computation," *Comput.-Aided Des.*, vol. 39, no. 8, pp. 625–638, 2007.

[38] H. Edelsbrunner and J. Harer, *Computational Topology: An Introduction*. Providence, RI, USA: AMS, 2010.

[39] H. Edelsbrunner and D. Morozov, "Persistent homology: Theory and practice," Ernest Orlando Lawrence Berkeley Nat. Lab., Berkeley, CA, USA, Tech. Rep. LBNL-6037-E, 2012.

[40] S. Boyd and L. Vandenberghe, *Convex Optimization*. Cambridge, U.K.: Cambridge Univ. Press, 2004.

[41] C. Chen and M. Kerber, "Persistent homology computation with a twist," in *Proc. 27th Eur. Workshop Comput. Geometry*, vol. 11. 2011. [Online]. Available: http://research.cs.rutgers.edu/~cc1092/publications/chen_eurocg_2011.pdf

[42] *CGAL User and Reference Manual*, 4th ed. The CGAL Project, CGAL Editorial Board, 2015.

[43] D. Fiser. *Libccd—Collision Detection Between Convex Shapes*. Accessed: Apr. 1, 2015. [Online]. Available: http://libccd.danfis.cz/
[44] B. Calli, A. Walsman, A. Singh, S. Srinivasa, P. Abbeel, and A. M. Dollar. (2015). "Benchmarking in manipulation research: The YCB object and model set and benchmarking protocols." [Online]. Available: https://arxiv.org/abs/1502.03143
[45] W. Wohlkinger, A. Aldoma, R. B. Rusu, and M. Vincze, "3DNet: Large-scale object class recognition from cad models," in *Proc. IEEE Int. Conf. Robot. Autom. (ICRA)*, May 2012, pp. 5384–5391.
[46] M. Laskey *et al.*, "Robot grasping in clutter: Using a hierarchy of supervisors for learning from demonstrations," in *Proc. IEEE Conf. Autom. Sci. Eng. (CASE)*, Aug. 2016, pp. 827–834.
[47] J. Su, H. Qiao, Z. Ou, and Z. Y. Liu, "Vision-based caging grasps of polyhedron-like workpieces with a binary industrial gripper," *IEEE Trans. Autom. Sci. Eng.*, vol. 12, no. 3, pp. 1033–1046, Jul. 2015.
[48] G. Van Den Bergen, "Proximity queries and penetration depth computation on 3D game objects," in *Proc. Game Develop. Conf.*, vol. 170. 2001. [Online]. Available: https://graphics.stanford.edu/courses/cs468-01-fall/Papers/van-den-bergen.pdf

Jeffrey Mahler (M'18) received the B.S. degree (Hons.) in electrical engineering from the University of Texas at Austin, Austin, TX, USA, in 2013. He is currently pursuing the Ph.D. degree in electrical engineering and computer sciences (with a specialization in robotics and artificial intelligence) with the University of California at Berkeley, Berkeley, CA, USA.

He co-founded the 3-D scanning company Lynx Laboratories in 2012, which was acquired by Occipital in 2015. His research interests include robust robot grasping, deep learning for robot perception, and imitation learning.

Mr. Mahler was awarded the the National Defense Science and Engineering Graduate Fellowship in 2015.

Florian T. Pokorny (M'18) received the B.Sc. degree in mathematics from the University of Edinburgh, Edinburgh, U.K., in 2005 and completed Part III of the Mathematical Tripos with the University of Cambridge, Cambridge, U.K., in 2006. He then received the Ph.D. degree in mathematics from the University of Edinburgh in 2011.

In 2011, he joined the KTH Royal Institute of Technology, Stockholm, Sweden, as a Post-Doctoral Researcher. From 2015 to 2016, he conducted Post-Doctoral Research with the AMPLab and the Berkeley Automation Science and Engineering Laboratory, University of California at Berkeley, Berkeley, CA, USA, under the supervision of Prof. K. Goldberg. He is currently an Assistant Professor with the Robotics, Perception and Learning Lab, KTH Royal Institute of Technology. His research interests include robotic manipulation, machine learning, and topological data analysis.

Sherdil Niyaz (M'18) received the B.S. degree in electrical engineering and computer sciences from the University of California at Berkeley, Berkeley, CA, USA, in 2017, where he researched grasping in the Autolab with Prof. K. Goldberg. He is currently pursuing the Ph.D. degree in computer science with the University of Washington, Seattle, WA, USA, working with Prof. S. Srinivasa on motion planning.

He is broadly interested in robotics, with a focus on manipulation.

Ken Goldberg (F'18) received the Ph.D. degree in computer science from Carnegie Mellon University, Pittsburgh, PA, USA, in 1990.

He is the William S. Floyd Distinguished Chair of Engineering and the Chair of the Industrial Engineering and Operations Research Department, University of California at Berkeley, Berkeley, CA, USA, with appointments in electrical engineering, computer science, art practice, and the School of Information. He has authored more than 250 refereed papers and holds eight U.S. patents.

Dr. Goldberg was a recipient of the NSF Presidential Faculty Fellowship in 1995, the Joseph Engelberger Award in 2000, and the IEEE Major Educational Innovation Award in 2001. He is the Founding Co-Chair of the IEEE Technical Committee on Networked Robots and the Founding Chair of the (T-ASE) Advisory Board. He served as the Editor-in-Chief for the IEEE TRANSACTIONS ON AUTOMATION SCIENCE AND ENGINEERING from 2011 to 2016 and served two terms from 2006 to 2009 as the Vice-President of Technical Activities for the IEEE Robotics and Automation Society.